This is a copy of the published version, or version of record, available on the publisher's website. This version does not track changes, errata, or withdrawals on the publisher's site.

Probing the superconducting ground state of noncentrosymmetric high-entropy alloys using muon-spin rotation and relaxation

Kapil Motla, Arushi, P. K. Meena, D. Singh, P. K. Biswas, A. D. Hillier, and R. P. Singh

Published version information

Citation: K Motla et al. Probing the superconducting ground state of noncentrosymmetric high-entropy alloys using muon-spin rotation and relaxation. Phys Rev B 104, no. 9 (2021): 094515

DOI: 10.1103/PhysRevB.104.094515

This version is made available in accordance with publisher policies. Please cite only the published version using the reference above. This is the citation assigned by the publisher at the time of issuing the APV. Please check the publisher's website for any updates.

This item was retrieved from **ePubs**, the Open Access archive of the Science and Technology Facilities Council, UK. Please contact epublications@stfc.ac.uk or go to http://epubs.stfc.ac.uk/ for further information and policies.

Probing the superconducting ground state of noncentrosymmetric high-entropy alloys using muon-spin rotation and relaxation

Kapil Motla,[1] Arushi,[1] P. K. Meena,[1] D. Singh,[2] P. K. Biswas,[2] A. D. Hillier,[2] and R. P. Singh[1,*]

[1]*Department of Physics, Indian Institute of Science Education and Research Bhopal, Bhopal 462066, India*

[2]*ISIS Facility, STFC Rutherford Appleton Laboratory, Harwell Science and Innovation Campus, Oxfordshire OX11 0QX, United Kingdom*

(Received 10 May 2021; revised 3 September 2021; accepted 7 September 2021; published 16 September 2021)

Recently, high-entropy alloys (HEAs) have emerged as a unique platform for discovering superconducting materials and offer avenues to explore exotic superconductivity. The highly disordered nature of HEAs suggests the regular phonon required for BCS superconductivity may be unlikely to occur. Therefore, understanding the microscopic properties of these superconducting HEAs is important. We report a detailed characterization of the superconducting properties of the noncentrosymmetric (α-Mn structure) HEAs $(HfNb)_{0.10}(MoReRu)_{0.90}$ and $(ZrNb)_{0.10}(MoReRu)_{0.90}$ by using magnetization, specific heat, AC transport, and muon-spin relaxation/rotation (μSR). Despite the disordered nature, low-temperature specific heat and transverse-field muon spin rotation measurements suggest a nodeless isotropic superconducting gap, and zero-field μSR measurements confirm that time reversal symmetry is preserved in the superconducting ground state.

DOI: 10.1103/PhysRevB.104.094515

I. INTRODUCTION

High-entropy alloys (HEAs) are a class of materials with tunable physical and superior mechanical properties compared to conventional binary and ternary alloys. These materials are getting widespread attention from many different scientific areas, including material science and theoretical and experimental condensed-matter physics [1–6]. HEAs are multicomponent alloys that contain five or more elements in near-equimolar ratios [7–10]. The Gibbs free energy decreases at high temperature and plays a vital role in crystallizing HEAs in different crystallographic structures [2,11,12]. Recently, HEA superconductors have emerged as a class of disordered alloy superconductors, having a high superconducting transition temperature and critical field. Also, they show retention of superconductivity at very high pressure [13]. Superconductivity was first reported in the high-entropy alloy $Ta_{34}Nb_{33}Hf_8Zr_{14}Ti_{11}$ [14]; since then, it has been observed in a few others high-entropy alloys [15–21]. To date, most of the research in HEA superconductors has been focused on discovering new HEA superconducting materials that crystallize in various structures and enhance the superconducting transition temperature. In contrast, the superconducting pairing mechanism is largely unexplored, mainly due to the HEA multicomponent and a high-disorder nature. It is difficult to calculate the electronic structure and understand the lattice vibration, which are usually essential for understanding the superconducting pairing mechanism. A comparative study of binary alloy superconductors with HEAs, which have the same crystal structure and a large disorder, can provide more insight into the superconducting properties of HEAs. A topical example of a binary alloy is the Re-based superconductors. These materials have a noncentrosymmetric α-Mn crystal structure and have been studied extensively due to the presence of time reversal symmetry (TRS) breaking [22–26]. However, the exact superconducting pairing mechanism is still not fully understood. Structural similarity, disorder, and the multicomponent nature of Re-based noncentrosymmetric (NCS) HEAs may help us understand the superconducting pairing mechanism of noncentrosymmetric superconducting compounds and HEAs themselves, which are still elusive. In this paper, we perform a comprehensive study of the superconducting ground state using magnetization, heat capacity, and resistivity, together with muon-spin spectroscopy on the NCS α-Mn HEA $(HfNb)_{0.10}(MoReRu)_{0.90}$, having a $T_C = 5.9(1)$ K, and another α-Mn NCS HEA, $(ZrNb)_{0.10}(MoReRu)_{0.90}$, reported by Stolze *et al.* [18], having a T_C 5.8(1) K.

II. EXPERIMENTAL DETAILS

Polycrystalline samples of the $(HfNb)_{0.10}(MoReRu)_{0.90}$ and $(ZrNb)_{0.10}(MoReRu)_{0.90}$ HEAs were prepared by arc melting stoichiometric quantities of high-purity elements (5N) under argon (5N) atmosphere. The resulting ingots were flipped and melted several times to enhance the homogeneity. In both HEAs, the weight loss was negligible (<0.1%) after melting. Phase purity and crystal structure of the samples were confirmed by x-ray diffraction at room temperature on a PANalytical diffractometer equipped with Cu $K\alpha$ radiation ($\lambda = 1.54056$ Å).

Temperature- and field-dependent magnetization, heat capacity, and transport measurements were performed using a Quantum Design MPMS-3 and physical property measurement system. The muon-spin relaxation/rotation (μSR) measurements in zero-field (ZF) and transverse-field (TF) conditions were carried out using the MuSR spectrometer at

*rpsingh@iiserb.ac.in

 ©2021 American Physical Society

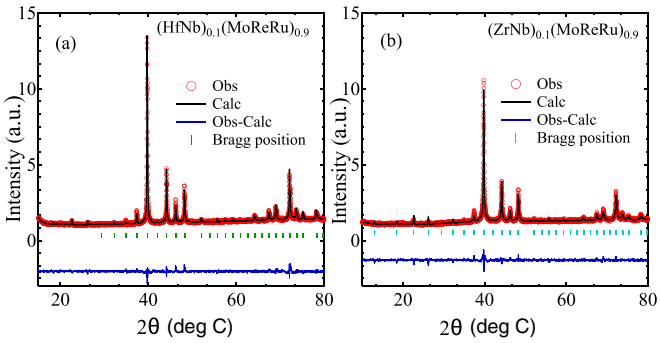

FIG. 1. The x-ray diffraction pattern from $(HfNb)_{0.10}(MoReRu)_{0.90}$ (left) and $(ZrNb)_{0.10}(MoReRu)_{0.90}$ (right) collected at room temperature using Cu $K\alpha$ radiation ($\lambda = 1.54056$ Å). The black line is the Le Bail fitting, and the green ticks are the expected locations for the diffraction Bragg peaks.

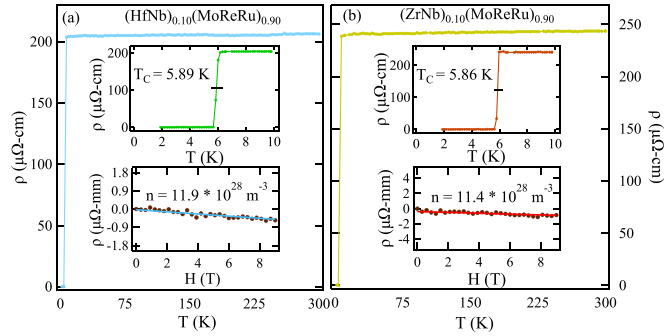

FIG. 2. Temperature dependence of the resistivity for (a) $(HfNb)_{0.10}(MoReRu)_{0.90}$ and (b) $(ZrNb)_{0.10}(MoReRu)_{0.90}$ in zero field. The top insets show the superconducting transition, and the bottom insets show the field-dependent Hall resistivity at 10 K.

the ISIS Neutron and Muon Facility, Rutherford Appleton Laboratory, United Kingdom. A full description of the μSR technique may be found in Ref. [27].

III. RESULTS

A. Structural characterization

X-ray diffraction spectra from both HEAs were collected at ambient conditions, and Le Bail fitting was carried out using the FULLPROF software [28], as shown in Fig. 1. Figure 1 shows that both alloys crystallize in a cubic noncentrosymmetric α-Mn (space group $I\bar{4}3m$) crystal structure and have unit cell parameters $a =$ 9.6170(2) Å and 9.6180(2) Å for $(HfNb)_{0.10}(MoReRu)_{0.90}$ and $(ZrNb)_{0.10}(MoReRu)_{0.90}$, respectively. The refined cell parameters of $(ZrNb)_{0.10}(MoReRu)_{0.90}$ are in good agreement with the published data [18]. Due to the large number of different atoms and sites, the tendency to form a solid solution makes it difficult to determine the occupancies of atomic sites unambiguously (see the Supplemental Material [29]).

B. Normal and superconducting state properties

1. Electrical resistivity

Temperature dependences of the resistivity $\rho(T)$ for both samples were performed in zero field from 1.9 to 300 K. The results for $(HfNb)_{0.10}(MoReRu)_{0.90}$ and $(ZrNb)_{0.10}(MoReRu)_{0.90}$ are shown in Figs. 2(a) and 2(b), respectively. Low-temperature data shown in the top insets in Figs. 2(a) and 2(b) clearly present a very sharp drop in resistivity at $T_C^{mid} = 5.9(1)$ and 5.8(1) K for $(HfNb)_{0.10}(MoReRu)_{0.90}$ and $(ZrNb)_{0.10}(MoReRu)_{0.90}$, respectively. Resistivity increases leisurely with temperature, showing poor metallic behavior. The residual resistivity ratio (RRR) for both samples was found to be 1.2. The small value of the RRR for both HEAs indicates a high degree of disorder, and these values are comparable to the reported RRR ratio for HEAs and α-Mn binary alloys [18,23–25,30]. A Hall measurement was also performed to calculate the carrier concentration and the type of charge carriers. The bottom insets in Figs. 2(a) and 2(b) show the field dependence of Hall resistivity ρ measured at $T = 10$ K for both HEAs. $\rho(H)$ is well described by a straight line fit, and carrier concentration yields $n = 11.9(4) \times 10^{-28}$ m^{-3} and $11.4(8) \times 10^{-28}$ m^{-3}, respectively, for $(HfNb)_{0.10}(MoReRu)_{0.90}$ and $(ZrNb)_{0.10}(MoReRu)_{0.90}$.

2. Magnetization

To confirm bulk superconductivity in both HEAs, the temperature dependence of the DC magnetization measurements was measured in an applied field of 1.0 mT in zero-field-cooled warming (ZFCW) and field-cooled cooling (FCC) modes. The onset of superconductivity was observed below $T_C = 5.2(1)$ K for $(HfNb)_{0.10}(MoReRu)_{0.90}$ and 5.5(1) K for $(ZrNb)_{0.10}(MoReRu)_{0.90}$ by a sharp decrease in a diamagnetic magnetization, as shown in Figs. 3(a) and 3(e). In order to estimate the lower critical field H_{C1}, we have performed magnetization versus field measurements at a range of temperatures. The value of H_{C1} at each temperature is taken as the deviation of the magnetization from the linearity, as shown in the insets of Figs. 3(b) and 3(f) for $(HfNb)_{0.10}(MoReRu)_{0.90}$ and $(ZrNb)_{0.10}(MoReRu)_{0.90}$. The lower critical field at absolute zero temperature $H_{C1}(0)$ can be calculated by extrapolating H_{C1}(T) using the Ginzburg-Landau expression, which is given as

$$H_{C1}(T) = H_{C1}(0)(1 - t^2), \tag{1}$$

where $t = T/T_C$ and the lower critical field $H_{C1}(0)$ was estimated as 2.14(1) and 3.27(3) mT for $(HfNb)_{0.10}(MoReRu)_{0.90}$ and $(ZrNb)_{0.10}(MoReRu)_{0.90}$, respectively, by fitting Eq. (1) in the data given in Figs. 3(b) and 3(f).

The upper critical field at $T = 0$ K, $H_{C2}(0)$, is estimated using the Ginzburg-Landau (GL) relation

$$H_{C2}(T) = H_{C2}(0)\left(\frac{(1 - t^2)}{(1 + t^2)}\right), \tag{2}$$

where $t = T/T_C$ and the estimated value of $H_{C2(res,mag,hc)}(0)$ = 8.7(1), 9.4(1), and 9.7(1) T for $(HfNb)_{0.10}(MoReRu)_{0.90}$ and $H_{C2(Res,mag)}(0)$ = 10.4(9) and 11.5(2) T for $(ZrNb)_{0.10}(MoReRu)_{0.90}$. The Ginzburg-Landau coherence length (the length between Cooper pairs) can be estimated with the help of $H_{C2}(0)$ by using the expression

$$H_{C2}(0) = \frac{\Phi_0}{2\pi\xi_{GL}^2}, \tag{3}$$

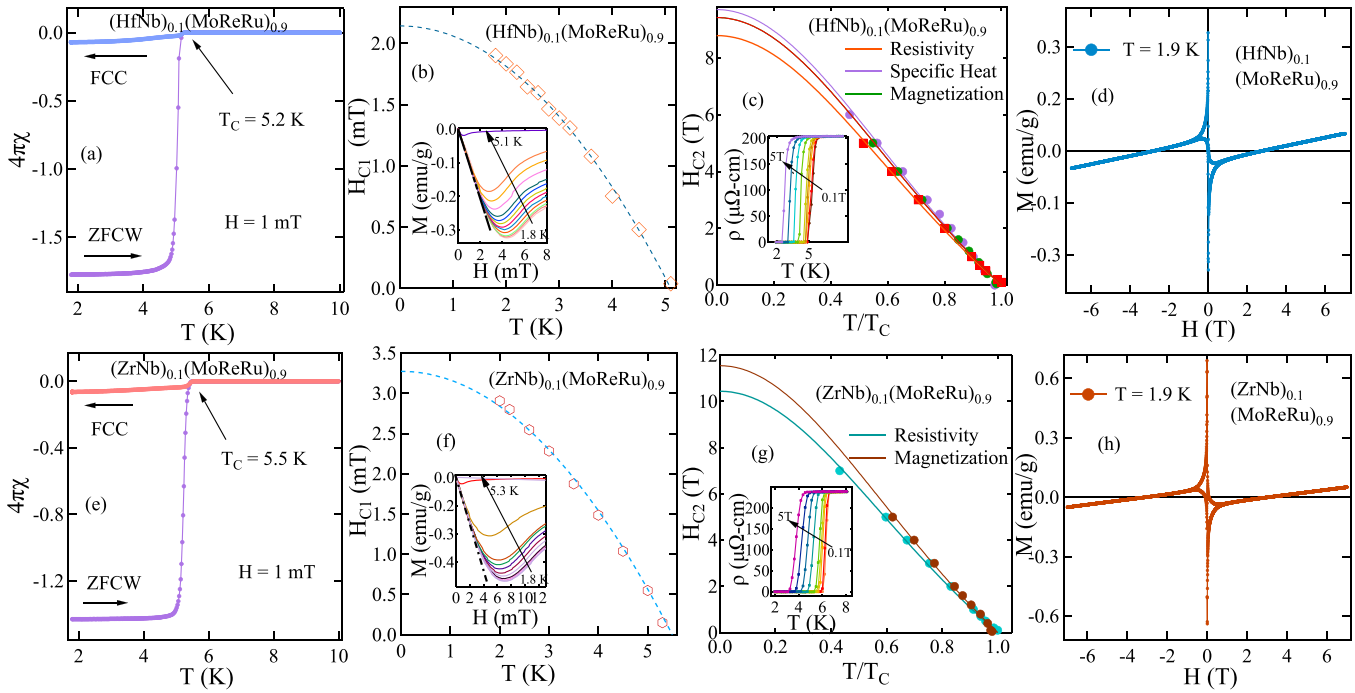

FIG. 3. (a) and (e) The temperature dependence of magnetic moment in 1.0 mT in FCC and ZFCW modes. (b) and (f) The temperature dependence of the lower critical field. (c) and (g) The upper critical field estimated using specific heat, resistivity, and magnetization data. The dotted lines are the result of the fit to Eq. (2). (d) and (h) Magnetic field dependent magnetization (M-H) at 1.9 K.

where Φ_0 is the flux quantum ($\Phi_0 = 2.07 \times 10^{-15}\,\mathrm{T\,m^2}$). Substituting the $H_{C2}(0)$ value from magnetization gives $\xi_{GL} = 5.92(2)$ nm for $(HfNb)_{0.10}(MoReRu)_{0.90}$ and 5.35(3) nm for $(ZrNb)_{0.10}(MoReRu)_{0.90}$. The calculated values of $H_{C1}(0)$ and $\xi_{GL}(0)$ were used to evaluate the magnetic penetration depth $\lambda_{GL}(0)$ (the value of the distance at which magnetic field becomes $1/e$ times the external applied magnetic field) for both the samples with the help of the relation

$$H_{C1}(0) = \frac{\Phi_0}{4\pi\lambda_{GL}^2(0)}\left(\ln\frac{\lambda_{GL}(0)}{\xi_{GL}(0)} + 0.12\right) \qquad (4)$$

and were obtained as 609(2) and 487(3) nm for $(HfNb)_{0.10}(MoReRu)_{0.90}$ and $(ZrNb)_{0.10}(MoReRu)_{0.90}$, respectively. The Ginzburg-Landau ratio is given by $\frac{\lambda_{GL}(0)}{\xi_{GL}(0)}$ and $\kappa_{GL} > \frac{1}{\sqrt{2}}$ for $(HfNb)_{0.10}(MoReRu)_{0.90}$ and $(ZrNb)_{0.10}(MoReRu)_{0.90}$, respectively. This confirms that both of these HEAs are, indeed, strong type II superconductors.

In a type II superconductor, Cooper pair breaking due to the applied magnetic field is attributed to two types of mechanisms: the orbital limiting field and Pauli paramagnetic limiting field effect [31,32]. In the orbital pair breaking, the induced kinetic energy of a Cooper pair by an external field exceeds the Cooper pair condensation energy. However, in Pauli limiting, the applied magnetic field aligns one of the Cooper pair spin moments in the direction of its field, thereby breaking the pairing. The orbital limiting field $H_{C2}^{\mathrm{orbital}}(0)$ is given by the Werthamar-Helfand-Hohenberg expression:

$$H_{C2}^{\mathrm{orbital}}(0) = -\alpha T_C \left.\frac{dH_{C2}(T)}{dT}\right|_{T=T_C}, \qquad (5)$$

where α is the purity factor and a value of 0.693 defines dirty-limit superconductors (see Sec. III B 5). The initial slope $-\frac{dH_{C2}}{dT}$ at $T = T_C$ was estimated 2.24(5) and 2.6(2) T/K for $(HfNb)_{0.10}(MoReRu)_{0.90}$ and $(ZrNb)_{0.10}(MoReRu)_{0.90}$, respectively, and gives the orbital limiting upper critical field $H_{C2}^{orb}(0)$ as 8.0(2) T for $(HfNb)_{0.10}(MoReRu)_{0.90}$ and 9.9(5) T for $(ZrNb)_{0.10}(MoReRu)_{0.90}$. The Pauli paramagnetic limit is given by $H_{C2}^{P} = 1.84\,T_C$ within the BCS theory. Substituting the values of T_C, we have determined $H_{C2}^{P} = 9.56(2)$ and 10.12(2) T for $(HfNb)_{0.10}(MoReRu)_{0.90}$, and $(ZrNb)_{0.10}(MoReRu)_{0.90}$, respectively. The Maki parameter, which is a measure of the strength of the Pauli limiting field and orbital critical field, is given by the expression $\alpha_M = \sqrt{2}H_{C2}^{orb}(0)/H_{C2}^{p}(0)$. The values obtained for α_M are 1.18 for $(HfNb)_{0.10}(MoReRu)_{0.90}$ and 1.38 for $(ZrNb)_{0.10}(MoReRu)_{0.90}$.

The magnetization hysteresis loops for both HEAs at 1.9 K are shown in Figs. 3(d) and 3(h). A closed-loop form at 2.0 and 3.5 T denotes that H_{irr} is far below the upper critical magnetic fields of both HEA samples. These values of H_{irr} suggest the depinning of the flux line vortices. The depinning generally happens due to the thermal fluctuation of the condensation energy of the Cooper pair or is stress induced by the grain boundary/disorder in polycrystalline samples. The strength of the thermal fluctuation with respect to the condensation energy of the charge carriers is described by the G_i number [33]. The calculated value of G_i for both HEAs ($\sim 10^{-5}$) falls between high T_C ($\sim 10^{-2}$) and conventional superconductors ($\sim 10^{-8}$), suggesting the defect and grain boundaries could be responsible for depinning [34].

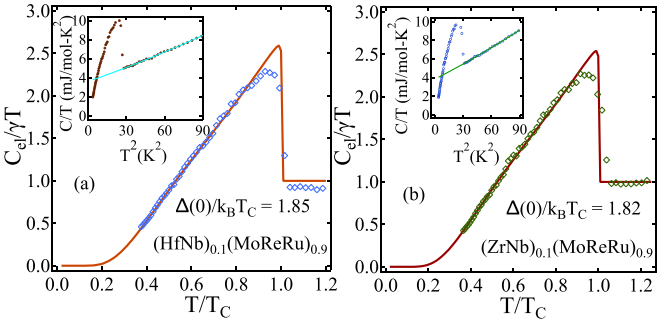

FIG. 4. Normalized specific heat data $C_{el}/\gamma_n T$ fitted with the BCS *s*-wave model shown by the red line for both HEAs: (a) $(HfNb)_{0.10}(MoReRu)_{0.90}$ and (b) $(ZrNb)_{0.10}(MoReRu)_{0.90}$. The inset shows the temperature-dependent specific heat data in zero-field data plotted as C/T vs T^2.

3. Specific heat

Specific heat measurements for both samples were performed between 1.9 and 20 K in zero field. The observed T_C for both the samples is in agreement with the magnetization and resistivity data. The specific heat data above T_C in the normal region were fitted using the equation $\frac{C}{T} = \gamma_n + \beta_3 T^2 + \beta_5 T^4$ and are shown in the insets in Fig. 4. Here γ_n is the coefficient for electronic specific heat in the normal state (Sommerfeld coefficient) and β_3 and β_5 are the phononic contributions. The fitting provides the parameters as $\gamma_n =$ 3.6(1) and 3.8(1) mJ mol^{-1} K^{-2}, $\beta_3 = 0.047(1)$ and 0.052(3) mJ mol^{-1} K^{-4}, and $\beta_5 = 0.07(1)$ and 0.07(1) μJ mol^{-1} K^{-6} for $(HfNb)_{0.10}(MoReRu)_{0.90}$ and $(ZrNb)_{0.10}(MoReRu)_{0.90}$, respectively.

The density of states $D_C(E_F)$ and Debye temperature θ_D have been calculated using γ_n and β_3. The obtained values are $D_C(E_F) = 1.53(3)$ and 1.63(4) states/eV f.u. and $\theta_D = 346(2)$ and 335(7) K for $(HfNb)_{0.10}(MoReRu)_{0.90}$ and $(ZrNb)_{0.10}(MoReRu)_{0.90}$, respectively. Moreover, the strength of the attractive interaction between the electron and phonon can be expressed according to the McMillan model [35] as

$$\lambda_{e-\mathrm{ph}} = \frac{1.04 + \mu^* \ln(\theta_D/1.45T_C)}{(1 - 0.62\mu^*)\ln(\theta_D/1.45T_C) - 1.04}, \tag{6}$$

where μ^* is the screened Coulomb repulsion parameter, which is usually between 0.1 and 0.15 and for intermetallic superconductors is ~0.13 [24,25]. Inserting the value of the Debye temperature θ_D and T_C, we find the strength between the electron and phonon, $\lambda_{e-\mathrm{ph}} = 0.62(6)$ and 0.63(8), for $(HfNb)_{0.10}(MoReRu)_{0.90}$ and $(ZrNb)_{0.10}(MoReRu)_{0.90}$, respectively. This value indicates a moderately coupled superconductivity similar to other Re-based noncentrosymmetric superconductors such as Re_6Hf [24] and Re_6Ti [25].

In order to determine the electronic specific heat contribution, we have subtracted the phononic contribution from the total specific heat: $C_{el} = C(T) - \beta_3 T^3 - \beta_5 T^5$. The normalized electronic specific heat jump is $\frac{\Delta C_e l}{\gamma_n T_C} = 1.67$ for $(HfNb)_{0.10}(MoReRu)_{0.90}$ and 1.49 for $(ZrNb)_{0.10}(MoReRu)_{0.90}$, which further suggests moderately coupled superconductivity for both these HEA samples. The electronic specific heat data below transition temperature T_C can be best fit with the single-gap BCS expression for normalized entropy S,

$$\frac{S}{\gamma_n T_C} = -\frac{6}{\pi^2}\left(\frac{\Delta(0)}{k_B T_C}\right)\int_0^\infty [f\ln(f) + (1-f)\ln(1-f)]dy, \tag{7}$$

where $f(\xi) = \{\exp[E(\xi)/k_B T] + 1\}^{-1}$ is the Fermi function, with $E(\xi) = \sqrt{\xi^2 + \Delta^2(t)}$, where $E(\xi)$ is the energy of the normal electrons relative to the Fermi energy; $y = \xi/\Delta(0)$; $t = T/T_C$; and $\Delta(t) = \tanh(1.82\{1.018[(1/t) - 1]\}^{0.51})$ is the BCS approximation for the temperature dependence of the energy gap. The normalized electronic specific heat below T_C is related to the normalized entropy by

$$\frac{C_{el}}{\gamma_n T_C} = t\frac{d(S/\gamma_n T_C)}{dt}. \tag{8}$$

Figure 4 shows the fits of Eq. (8) to the specific heat data and provides $\frac{\Delta(0)}{k_B T_C} = 1.85(3)$ and 1.82(2) for $(HfNb)_{0.10}(MoReRu)_{0.90}$ and $(ZrNb)_{0.10}(MoReRu)_{0.90}$, respectively, both of which are higher than the usual BCS value in the weak-coupling limit, again suggesting moderately coupled superconductivity in both HEAs.

4. Muon spin relaxation and rotation

The nature of the superconducting ground state of both HEAs, $(HfNb)_{0.10}(MoReRu)_{0.90}$ and $(ZrNb)_{0.10}(MoReRu)_{0.90}$, was further investigated by using muon spin relaxation and rotation measurements. First, we shall discuss the ZF-μSR measurements, which were carried out above and below T_C for both samples. This was to detect any possibility of the presence of a time reversal symmetry breaking signal. The absence of any precession signal confirms the absence of local magnetic field associated with long-range ordering, and depolarization of muon spin occurs due to the presence of static randomly oriented nuclear moments. In the absence of magnetic moment, the behavior of time-dependent muon asymmetry spectra is best described by the Gaussian Kubo-Toyabe function [36]

$$G_{\mathrm{KT}}(t) = \frac{1}{3} + \frac{2}{3}(1 - \sigma_{\mathrm{ZF}}^2 t^2)\exp\left(\frac{-\sigma_{\mathrm{ZF}}^2 t^2}{2}\right), \tag{9}$$

where σ_{ZF} is the relaxation rate of the muon spin due to static, randomly oriented local fields associated with the nuclear moments. The time-dependent asymmetry spectra can be best described by the following function:

$$A(t) = A_1 G_{\mathrm{KT}}(t)\exp(-\Lambda t) + A_{\mathrm{BG}}, \tag{10}$$

where A_1 and A_{BG} are the sample asymmetry and nondecaying constant background signal and Λ is an electronic relaxation rate. ZF-μSR spectra collected in both normal and superconducting states exhibit the identical relaxations seen in overlapping ZF-μSR spectra (Fig. 5). They confirm additional ZF-μSR relaxations below the superconducting transition temperature exclude the possibility of time reversal symmetry in the superconducting ground state of both the HEAs.

To gain information on the superconducting gap structure, we have performed a TF-μSR measurement where an applied magnetic field of 30 mT was applied above the superconducting transition temperature and then the sample was cooled

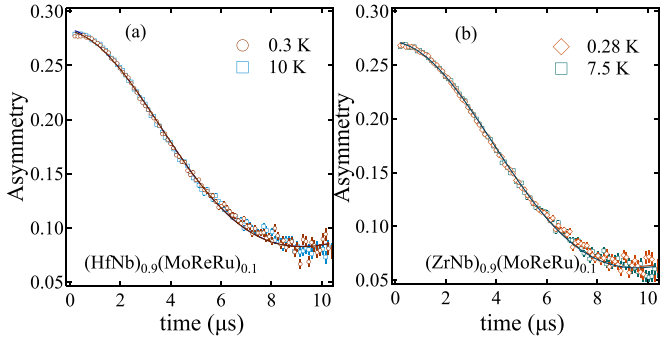

FIG. 5. Temperature-dependent ZF-μSR asymmetry spectra collected above and below the transition temperature for both samples. The fitting curve is shown as a solid line.

to the base temperature of 0.26 K of the ^{3}He cryostat. The applied magnetic field is greater than H_{C1} but less than H_{C2} in order to generate a flux line lattice. Figure 6 shows the TF-μSR asymmetry spectra below and above T_C for both HEAs. The fast decay of TF-μSR spectra below T_C with respect to spectra above T_C is due to the formation of the flux lattice line. The TF-μSR signal is best fit with the oscillatory function:

$$A(t) = \sum_{i=1}^{N} A_i \exp\left(-\frac{1}{2}\sigma_i^2 t^2\right)\cos(\gamma_\mu B_i t + \phi) + A_{\rm BG}\cos(\gamma_\mu B_{\rm BG} t + \phi), \quad (11)$$

where B_i is the mean field of the ith component of the Gaussian distribution, $B_{\rm BG}$ is the contribution from the sample holder, A_i and $A_{\rm BG}$ are the asymmetry contributions from the sample and sample holder, ϕ is the initial phase offset, and σ is the Gaussian muon spin depolarization rate. The second moment was used in the case of $(HfNb)_{0.10}(MoReRu)_{0.90}$, and the first and second moments are given as

$$B = \sum_{i=1}^{2} \frac{A_i B_i}{A_1 + A_2}, \quad (12)$$

$$\langle \Delta B^2 \rangle = \frac{\sigma^2}{\gamma_\mu^2} = \sum_{i=1}^{2} \frac{A_i[(\sigma_i/\gamma_\mu)^2 + (B_i - B)^2]}{A_1 + A_2}. \quad (13)$$

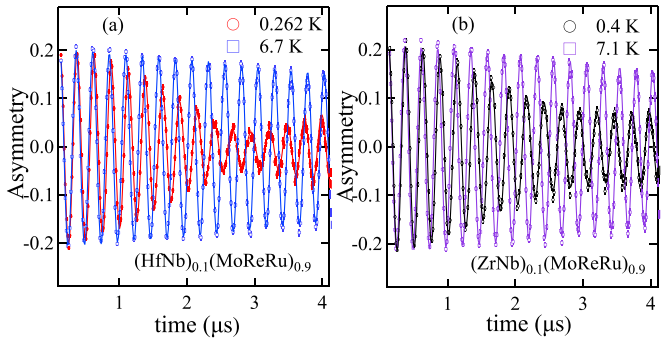

FIG. 6. Transverse field asymmetry spectra were collected at 30 mT magnetic field above and below the transition temperature of HEAs. The solid line is the fit using the Gaussian modulated oscillatory function.

TABLE I. Superconducting and normal state parameters of $(HfNb)_{0.10}(MoReRu)_{0.90}$ (Hf-HEA) and $(ZrNb)_{0.10}(MoReRu)_{0.90}$ (Zr-HEA)

Parameter	Units	Hf-HEA	Zr-HEA
T_C	K	5.2(1)	5.5(1)
$H_{C1}(0)$	mT	2.1(1)	3.2(3)
$H_{C2}^{mag}(0)$	T	9.4(1)	11.5(2)
$H_{C2}^{P}(0)$	T	9.56(3)	10.12(3)
$\xi_{\rm GL}$	nm	5.92(2)	5.35(3)
$\lambda_{\rm GL}$	nm	609(2)	487(3)
$\lambda(0)_{muon}$	nm	495(6)	522(1)
$k_{\rm GL}$		103(1)	91(1)
$\Delta C_{el}/\gamma_n T_C$		1.67(5)	1.49(4)
$\Delta(0)/k_B T_C$ (specific heat)		1.85(3)	1.82(2)
$\Delta(0)/k_B T_C$ (muon)		1.68(6)	1.96(8)
m^*/m_e		4.7(2)	5.3(2)
v_F	10^5 m s^{-1}	3.7(2)	3.2(2)
n_s	10^{28} m^{-3}	11.9(4)	11.4(8)
ξ_0/l_e		374(98)	332(93)

σ includes both the temperature-independent depolarization σ_N, which comes from the static field arising due to the nuclear magnetic moment, and the contribution of the field variation from the flux line lattice, given as $\sigma^2 = \sigma_N^2 + \sigma_{\rm FLL}^2$. As for both the samples $\xi(0)/l > 1$ (see Table I), the temperature-dependent London magnetic penetration depth in the dirty limit within the London approximation can be estimated by

$$\frac{\sigma_{\rm FLL}(T)}{\sigma_{\rm FLL}(0)} = \frac{\lambda^{-2}(T)}{\lambda^{-2}(0)} = \frac{\Delta(T)}{\Delta(0)}\tanh\left[\frac{\Delta(T)}{2k_B T}\right]. \quad (14)$$

The solid line in Fig. 7 is the fit, using Eq. (14), to the muon depolarization rate from the flux line lattice, which reveals the values of the energy gap as $\Delta(0) = 0.75(3)$ meV $[\Delta(0)/k_B T_C = 1.68(6)]$ for $(HfNb)_{0.10}(MoReRu)_{0.90}$ and $\Delta(0) = 0.95(1)$ meV $[\Delta(0)/k_B T_C = 1.96(8)]$ for $(ZrNb)_{0.10}(MoReRu)_{0.90}$. These values are in good agreement with the values obtained from specific heat data. For a high $H_{c2}(0)$ superconductor, the muon spin

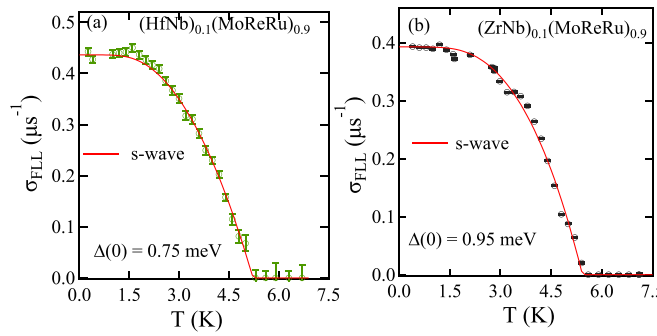

FIG. 7. TF field muon depolarization data collected at 30 mT. The data are well described using an isotropic s-wave model for both $(HfNb)_{0.10}(MoReRu)_{0.90}$ (left) and $(ZrNb)_{0.10}(MoReRu)_{0.90}$ (right).

relaxation rate in the superconducting state σ_{FLL} is related to the London penetration depth λ via [37,38]

$$\frac{\sigma_{\mathrm{FLL}}^2(T)}{\gamma_\mu^2} = \frac{0.00371\Phi_0^2}{\lambda^4(T)}, \tag{15}$$

where $\gamma_\mu/2\pi = 135.5\,\mathrm{MHz/T}$ is the muon gyromagnetic ratio and Φ_0 is the magnetic flux quantum. Within the London approximation, the estimated values of $\lambda(0)$ are 495(6) and 522(1) nm for $(\mathrm{HfNb})_{0.10}(\mathrm{MoReRu})_{0.90}$ and $(\mathrm{ZrNb})_{0.10}(\mathrm{MoReRu})_{0.90}$, respectively.

5. Discussion

To supplement the results of the experimental measurements, we have performed calculations of the electronic properties. The electronic heat coefficient γ_n is directly dependent on the effective mass m^* and carrier density n of the quasiparticle via the expression [39]

$$\gamma_n = \left(\frac{\pi}{3}\right)^{2/3} \frac{k_B^2 m^* n^{1/3}}{\hbar^2}, \tag{16}$$

where k_B is Boltzmann's constant, using the electronic heat coefficients $\gamma_n = 3.6(1)$ and 3.8(1) mJ mol^{-1} K^{-2} (determined from the normal state heat capacity) and carrier densities $n = 11.9(4)$ and $11.4(8) \times 10^{28}\mathrm{m}^{-3}$ (obtained by Hall measurement) for $(\mathrm{HfNb})_{0.10}(\mathrm{MoReRu})_{0.90}$ and $(\mathrm{ZrNb})_{0.10}(\mathrm{MoReRu})_{0.90}$, respectively. This yields effective masses $m^* = 4.7(2)m_e$ and $5.3(2)m_e$, respectively, for $(\mathrm{HfNb})_{0.10}(\mathrm{MoReRu})_{0.90}$ and $(\mathrm{ZrNb})_{0.10}(\mathrm{MoReRu})_{0.90}$. The carrier density n and effective mass m^* of the quasiparticle are related to the Fermi velocity v_F by

$$n = \frac{1}{3\pi^2}\left(\frac{m^* v_{\mathrm{f}}}{\hbar}\right)^3, \tag{17}$$

which gives Fermi velocities of $v_F = 3.7(2)$ and $3.2(2) \times 10^5$ m/s for $(\mathrm{HfNb})_{0.10}(\mathrm{MoReRu})_{0.90}$ and $(\mathrm{ZrNb})_{0.10}(\mathrm{MoReRu})_{0.90}$, respectively. The mean free path l is related to the residual resistivity ρ_0, effective mass m^*, and Fermi velocity v_F of the quasiparticle as

$$l = \frac{3\pi^2\hbar^3}{e^2\rho_0 m^{*2} v_{\mathrm{F}}^2}. \tag{18}$$

Using the previously calculated value of the effective mass m^* and the Fermi velocity v_F with residual resistivity at the transition temperature $\rho_0 = 204(1)$ and $238(1)\,\mu\Omega$, cm (from the resistivity measurement), we obtain the electronic mean free paths $l = 2.6(2)$ and 2.4(5) Å for $(\mathrm{HfNb})_{0.10}(\mathrm{MoReRu})_{0.90}$ and $(\mathrm{ZrNb})_{0.10}(\mathrm{MoReRu})_{0.90}$, respectively. Within the BCS theory, the coherence length ξ_0 can be expressed in terms of Fermi velocity v_F and transition temperature T_C as

$$\xi_0 = \frac{0.18\hbar v_F}{k_B T_C}, \tag{19}$$

where k_B is Boltzmann's constant; v_F and T_C (from magnetization) are the Fermi velocity and transition temperature, from which we get $\xi_0 = 974(71)$ and 797(64) Å; and the ratio $\xi_0/l > 1$ for both $(\mathrm{HfNb})_{0.10}(\mathrm{MoReRu})_{0.90}$ and $(\mathrm{ZrNb})_{0.10}(\mathrm{MoReRu})_{0.90}$, which clearly suggests the signature

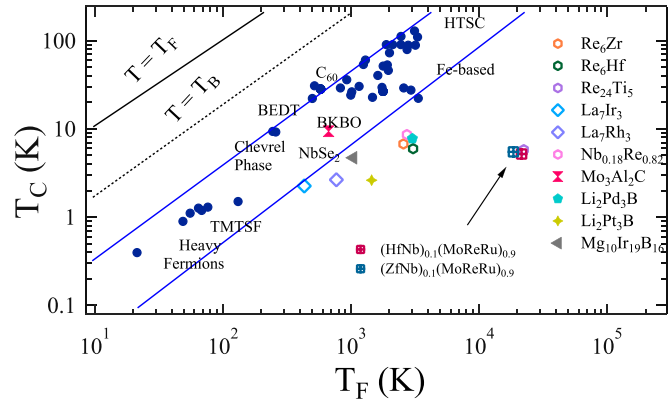

FIG. 8. Plot of the superconducting transition temperature versus Fermi temperature for different superconducting families. The two solid blue lines show the unconventional band of superconductors with other exotic superconductors [43–46] and lie near the unconventional band. $(\mathrm{HfNb})_{0.10}(\mathrm{MoReRu})_{0.90}$ and $(\mathrm{ZrNb})_{0.10}(\mathrm{MoReRu})_{0.90}$ are shown by red and blue squares, which lie far from the other unconventional superconductors.

of the dirty-limit superconductivity for both the HEA samples. The calculated parameters are listed in Table I.

Uemura *et al.* [40–42] classified the superconductor into conventional and unconventional in relation to the ratio of the superconducting temperature to the Fermi temperature. If this ratio value falls in the range $0.01 \leqslant T_c/T_F \leqslant 0.1$, then a superconductor is considered an unconventional one; the heavy-fermion superconductor, high-T_C superconductor, organic superconductor, and Fe-based superconductor lie inside this band. To calculate the T_F value for both HEA samples, the expression used is as follows: $k_B T_F = \frac{\hbar^2}{2m^*}(3\pi^2 n)^{2/3}$, where m^*, k_B, and n are the effective mass, Boltzmann's constant, and carrier density, respectively. The estimated values of T_F for $(\mathrm{HfNb})_{0.10}(\mathrm{MoReRu})_{0.90}$ and $(\mathrm{ZrNb})_{0.10}(\mathrm{MoReRu})_{0.90}$ are 21520(1480) and 18589(1445) K. T_C/T_F are far from the boundary of the unconventional superconductor as shown in Fig. 8, like the other noncentrosymmetric and unconventional superconductors.

IV. CONCLUSION AND SUMMARY

In conclusion, we have performed a full characterization of the superconducting properties of the NCS HEAs, in particular, $(\mathrm{HfNb})_{0.10}(\mathrm{MoReRu})_{0.90}$ and $(\mathrm{ZrNb})_{0.10}(\mathrm{MoReRu})_{0.90}$, by using μSR, magnetization, transport, and heat capacity measurements. It confirms bulk superconductivity, and $H_{C2}(0)$ is close to the Pauli limiting field, like in other Re-based NCS superconductors. The specific heat and TF-μSR measurements suggest moderately coupled superconductivity with the isotropic superconducting gap. The ZF-μSR result indicates time reversal symmetry is preserved in the superconducting ground state for both HEAs. In comparison the superconducting parameter of the NCS HEAs and the binary Re-based compounds (except for the preserved time reversal symmetry in the superconducting ground state) are surprisingly similar. The preserved TRS in the Re-based HEA superconducting ground state, despite structural and superconducting properties' similarity to the $\mathrm{Re_6}X$ series

of compounds, indicates the complex interplay of disorder and Re in the presence and absence of TRS breaking in the superconducting ground state. The similarity to binary superconductors and very low heat capacity value (in the range of elements) in multicomponent HEAs warrant further microscopic studies of more superconducting HEAs to understand whether all superconducting HEA alloys show similar behavior or HEAs with α-Mn crystal structure are unique.

ACKNOWLEDGMENTS

K.M. acknowledges the Council of Scientific and Industrial Research (CSIR), Government of India, for providing a SRF Fellowship (Award No. 09/1020(0123)/2017-EMR-I). R.P.S. acknowledges the Science and Engineering Research Board, Government of India, for Core Research Grant No. CRG/2019/001028. We thank ISIS, STFC, United Kingdom, for the beam time to perform the μSR experiments [47].

[1] M.-H. Tsai and J.-W. Yeh, Mater. Res. Lett. **2**, 107 (2014).
[2] Y. F. Ye, Q. Wang, J. Lu, C. T. Liu, and Y. Yang, Mat. Today **19**, 349 (2016).
[3] Z. Li, K. G. Pradeep, Y. Deng, D. Raabe, and C. C. Tasan, Nature (London) **534**, 227 (2016).
[4] C. Lee, G. Song, M. C. Gao, R. Feng, P. Chen, J. Brechtl, Y. Chen, K. An, W. Guo, J. D. Poplawsky, S. Li, A. T. Samaei, W. Chen, A. Hu, H. Choo, and P. K. Liaw, Acta Mater. **160**, 158 (2018).
[5] Z. Fan, H. Wang, Y. Wu, X. J. Liu, and Z. P. Lu, RSC Adv. **6**, 52164 (2016).
[6] Y. Zhang, T. T. Zuo, Y. Q. Cheng, and P. K. Liaw, Sci. Rep. **3**, 1455 (2013).
[7] J. W. Yeh, S. K. Chen, S. J. Lin, J. Y. Gan, T. S. Chin, T. T. Shun, C. H. Tsau, and S. Y. Chang, Adv. Eng. Mater. **6**, 299 (2004).
[8] C. L. Tracy, S. Park, D. R. Rittman, S. J. Zinkle, H. Bei, M. Lang, R. C. Ewing, and W. L. Mao, Nat. Commun. **8**, 15634 (2017).
[9] D. B. Miracle and O. N. Senkov, Acta Mater. **122**, 448 (2017).
[10] O. N. Senkov, G. B. Wilks, J. M. Scott, and D. B. Miracle, Intermetallics **19**, 698 (2011).
[11] M. C. Troparevsky, J. R. Morris, P. R. C. Kent, A. R. Lupini, and G. M. Stocks, Phys. Rev. X **5**, 011041 (2015).
[12] J.-W. Yeh, JOM **65**, 1759 (2013).
[13] J. Guo, H. Wang, F. von Rohr, Z. Wang, S. Cai, Y. Zhou, K. Yang, A. Li, S. Jiang, Q. Wu, R. J. Cava, and L. Sun, Proc. Natl. Acad. Sci. USA **114**, 13144 (2017).
[14] P. Koželj, S. Vrtnik, A. Jelen, S. Jazbec, Z. Jagličić, S. Maiti, M. Feuerbacher, W. Steurer, and J. Dolinšek, Phys. Rev. Lett. **113**, 107001 (2014).
[15] J. Wu, B. Liu, Y. Cui, Q. Zhu, G. Xiao, H. Wang, S. Wu, G. Cao, and Z. Ren, Sci. China Mater. **63**, 823 (2020).
[16] B. Liu, J. Wu, Y. Cui, Q. Zhu, G. Xiao, S. Wu, G. Cao, and Z. Ren, Scr. Mater. **182**, 109 (2020).
[17] S. Marik, K. Motla, M. Varghese, K. P. Sajilesh, D. Singh, Y. Breard, P. Boullay, and R. P. Singh, Phys. Rev. Mater. **3**, 060602(R) (2019).
[18] K. Stolze, F. A. Cevallos, T. Kong, and R. J. Cava, J. Mater. Chem. C **6**, 10441 (2018).
[19] Y. Mizuguchi, Md. R. Kasem, and T. A. D. Matsuda, Mater. Res. Lett. **9**, 141 (2021).
[20] L. Sun and R. J. Cava, Phys. Rev. Mater. **3**, 090301 (2019).
[21] J. Kitagawa, S. Hamamoto, and N. Ishizu, Metals **10**, 1078 (2020).
[22] E. Bauer and M. Sigrist, *Non-centrosymmetric Superconductor: Introduction and Overview* (Springer, Heidelberg, 2012).
[23] R. P. Singh, A. D. Hillier, B. Mazidian, J. Quintanilla, J. F. Annett, D. M. Paul, G. Balakrishnan, and M. R. Lees, Phys. Rev. Lett. **112**, 107002 (2014).
[24] D. Singh, A. D. Hillier, A. Thamizhavel, and R. P. Singh, Phys. Rev. B **94**, 054515 (2016).
[25] D. Singh, Sajilesh K. P., J. A. T. Barker, D. McK. Paul, A. D. Hillier, and R. P. Singh, Phys. Rev. B **97**, 100505(R) (2018).
[26] S. K. Ghosh, M. Smidman, T. Shang, J. F. Annett, A. D. Hillier, J. Quintanilla, and H. Yuan, J. Phys.: Condens. Matter **33**, 033001 (2021).
[27] A. D. Hillier, J. S. Lord, K. Ishida, and C. Rogers, Philos. Trans. R. Soc. A **377**, 20180064 (2019).
[28] J. Rodríguez-Carajal, Phys. B (Amsterdam, Neth.) **192**, 55 (1993).
[29] See Supplemental Material at http://link.aps.org/supplemental/10.1103/PhysRevB.104.094515 for Rietveld refinement considering elements to be equally occupied on every Wycoff position.
[30] F. O. von Rohr, M. J. Winiarski, J. Tao, T. Klimczuk, and R. J. Cava, Proc. Natl. Acad. Sci. USA **113**, E7144 (2016).
[31] E. Helfand and N. R. Werthamer, Phys. Rev. **147**, 288 (1966).
[32] M. Clogston, Phys. Rev. Lett. **9**, 266 (1962).
[33] O. Prakash, A. Thamizhavel, and S. Ramakrishnan, Supercond. Sci. Technol. **28**, 115012 (2015).
[34] Y. Li, J. Garcia, G. Franco, J. Lu, K. Lu, B. Rong, B. Shafiq, N. Chen, Y. Liu, L. Liu, B. Song, Y. Wei, S. S. Johnson, Z. Luo, and J. Feng, J. Appl. Phys. **117**, 213912 (2015).
[35] W. L. McMillan, Phys. Rev. **167**, 331 (1968).
[36] R. Kubo and T. Toyabe, *Magnetic Resonance and Relaxation* (North-Holland, Amsterdam, 1967).
[37] J. E. Sonier, J. H. Brewer, and R. F. Kiefl, Rev. Mod. Phys. **72**, 769 (2000).
[38] E. H. Brandt, Phys. Rev. B **37**, 2349 (1988).
[39] M. Tinkham, *Introduction to Superconductivity* (McGraw-Hill, New York, 1996).
[40] Y. J. Uemura, V. J. Emery, A. R. Moodenbaugh, M. Suenaga, D. C. Johnston, A. J. Jacobson, J. T. Lewandowski, J. H. Brewer, R. F. Kiefl, S. R. Kreitzman, G. M. Luke, T. Riseman, C. E. Stronach, W. J. Kossler, J. R. Kempton, X. H. Yu, D. Opie, and H. E. Schone, Phys. Rev. B **38**, 909 (1988).
[41] Y. J. Uemura *et al.*, Phys. Rev. Lett. **62**, 2317 (1989).
[42] Y. J. Uemura, L. P. Le, G. M. Luke, B. J. Sternlieb, W. D. Wu, J. H. Brewer, T. M. Riseman, C. L. Seaman, M. B. Maple, M. Ishikawa, D. G. Hinks, J. D. Jorgensen, G. Saito, and H. Yamochi, Phys. Rev. Lett. **66**, 2665 (1991).

[43] J. A. T. Barker, B. D. Breen, R. Hanson, A. D. Hillier, M. R. Lees, G. Balakrishnan, D. McK. Paul, and R. P. Singh, Phys. Rev. B **98**, 104506 (2018).

[44] C. S. Lue, H. F. Liu, C. N. Kuo, P. S. Shih, J.-Y. Lin, Y. K. Kuo, M. W. Chu, T.-L. Hung, and Y. Y. Chen, Supercond. Sci. Technol. **26**, 055011 (2013).

[45] D. A. Mayoh, J. A. T. Barker, R. P. Singh, G. Balakrishnan, D. McK. Paul, and M. R. Lees, Phys. Rev. B **96**, 064521 (2017).

[46] S. Sundar, S. Salem-Sugui, Jr., M. K. Chattopadhyay, S. B. Roy, L. S. Sharath Chandra, L. F. Cohen and L. Ghivelder, Supercond. Sci. Technol. **32**, 055003 (2018).

[47] D. Singh *et al.*, New family of noncentrosymmetric (α-Mn) High-Entropy Alloy Superconductors, STFC ISIS Neutron and Muon Source, doi: 10.5286/ISIS.E.RB1920420 (2019).